Supporting Information

for

Chromophore Quench-Labeling: An Approach to Quantifying Catalyst Speciation as Demonstrated for (EBI)$ZrMe_2$/$B(C_6F_5)_3$-Catalyzed Polymerization of 1-Hexene

D. Luke Nelsen,[†] Bernie J. Anding,[†] Julie L. Sawicki,[†] Matthew D. Christianson,[‡] Daniel J. Arriola,[‡] and Clark R. Landis[†]*

[†]Department of Chemistry, University of Wisconsin-Madison, 1101 University Avenue, Madison, Wisconsin 53706, United States

[‡]The Dow Chemical Company, Building 1776, Midland, Michigan 48674

* corresponding author: landis@chem.wisc.edu

Table of Contents

Quench Efficiency S3

Weight-Average Molecular Weight Evolution S3

Further Comparison of RI and UV Signals S4

Error Analysis (cont.) S4

Unlabeled Quenching verses Catalyst Death Prior to Reaction S8

Fits of the Data Using Optimized Rate Constants S11

NMR Spectra S18

Illustration of the Active Site Count Sensitivity of UV-Detected Polymers Produced by Quench-Labeling S27

Data and Computed Average and Standard Deviations for Active Site Counts S27

Quench Efficiency

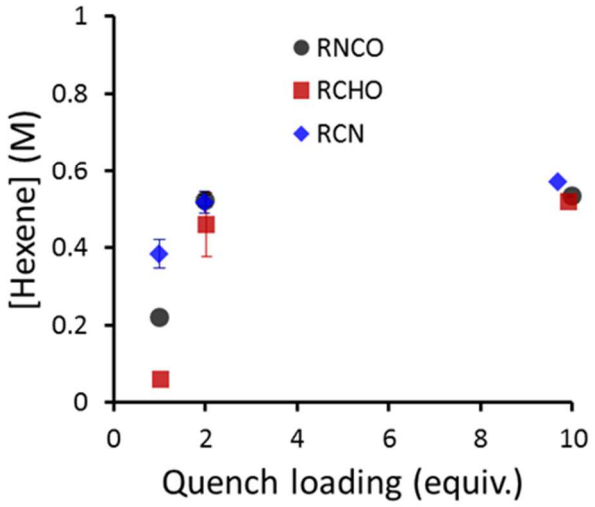

Figure S1. Monomer consumption as a function of quench loading for reactions conducted at 0 °C and quenched at 120 s ($[hexene]_0$ = 1.0 M and $[catalyst]_0$ = 2.17 mM). Lower monomer consumption values are indicative of incomplete quenching.

Weight-Average Molecular Weight Evolution

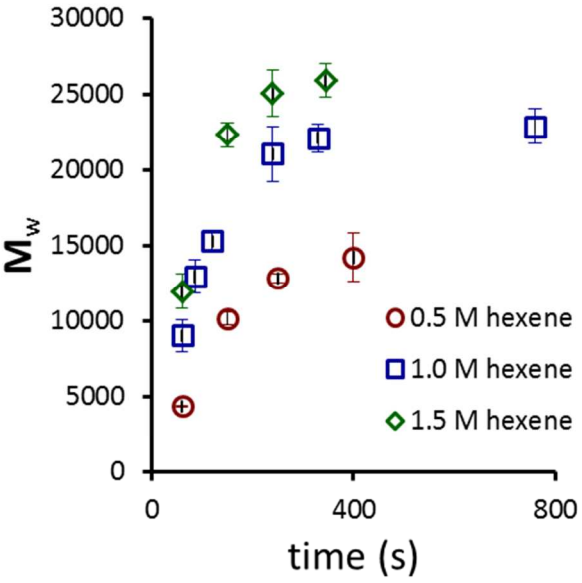

Figure S2. Time evolution of weight-average molecular weight for reactions run at 0 °C with $[catalyst]_0$ = 2.17 mM. Error bars represent 95% confidence for three duplicates.

Further Comparison of RI and UV Signals

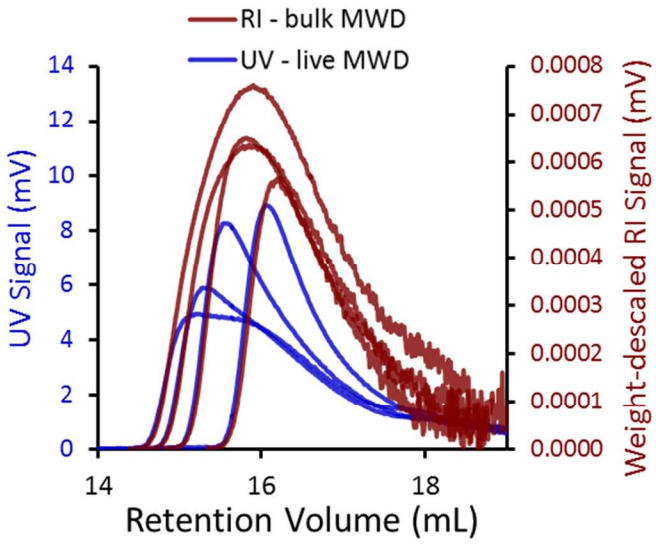

Figure S3. Overlap of UV and RI signals with RI signal de-scaled by polymer MW ([hexene]$_0$ = 1.0 M and [catalyst]$_0$ = 2.17 mM; 0 °C). With this treatment, both RI and UV are only concentration dependent. The obvious difference between RI and UV demonstrates that bulk MWD and live MWD are indeed distinct data.

Error Analysis

GPC Sample Concentration:

A polymer mass calibration curve was constructed for polyhexene using equation (S1), where c = concentration, A_{peak} = area of the RI signal, d_n/d_c = specific refractive index of polyhexene, and K(RI) = detector constant. A combined constant for the quotient of K(RI)/(d_n/d_c) was found to be 0.031 ± 0.003 (g/mL·μV). This value was used to determine the amount of polyhexene in the reaction samples, and the observed rate polymer concentrations closely coincided with the rate of monomer consumption, indicating that all polymer is detected by GPC and that monomer is not consumed by any non-polymerization side reactions. As a note, errors in GPC sample concentration do not affect modeling since all RI and UV data are normalized to the total area of the largest curve in each time course.

$$c = \frac{A_{peak}}{\left(d_n/d_c\right)} K(RI) \qquad \text{(S1)}$$

Accurate UV-GPC data is critical for the determination of active site counts. Treatment of UV data was accomplished in Excel, starting from the raw data in mV. All signals were processed by subtracting the dark spectrum and scaling by the background spectrum as is typically performed by modern-day spectrophotometer software. Chromophore concentration was calibrated for 7-pyrenyl-1-heptene using a standard Beer's Law plot.

To validate the data, two approaches for measuring active site counts were conducted concurrently for the UV-GPC data: (1) labeled polymer was determined as a fraction of total chromophore and (2) labeled polymer was quantified directly using the Beer's law calibration. Error bars for individual samples represent the deviance between the two approaches. In all cases, this deviance was equal to or less than the deviance between the

reaction duplicate samples. Averaging data from duplicate reactions was assumed sufficient in mitigating integration inconsistencies.

Molecular Weight Calibration and Retention Volume:

Daily relative molecular weight calibrations were accomplished using a five-point narrow polystyrene (PS) standard (EasiCal PS-2 from Polymer Laboratories (Varian)). An absolute molecular weight calibration for isotactic poly-(1-hexene) was determined previously, allowing for conversion of PS-equivalent molecular weights to poly-(1-hexene) molecular weights by the third-order polynomial shown in equation S2 where a = 0.072338628, b = -1.14026412, c = 7.076718034, and d = -10.95937204.[1]

$$Log\left(MW_{polyhexene}\right) = aLog(MW_{PS})^3 + bLog(MW_{PS})^2 + cLog(MW_{PS}) + d \qquad \text{(S2)}$$

Theoretically, verification of the absolute molecular weight is possible for this system since all polymer end-groups (active sites, vinylidene, and vinylene) and total incorporated monomer have been quantified. Molecular weights calculated by this method generally agree with the absolute molecular weights observed by GPC, but errors associated with end-group quantification are exacerbated, leading to large deviances in the calculated value and limiting the reliability of validation.

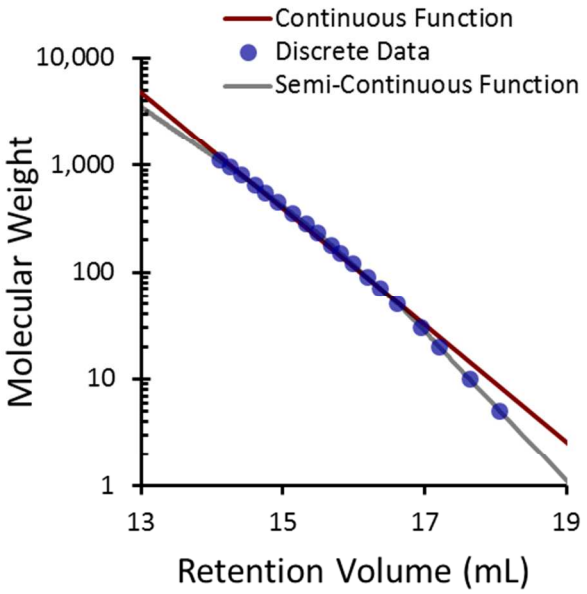

Figure S4: Relationship of retention volume to log of the molecular weight: fitting the discrete data points with continuous and semi-continuous functions.

Conversion of retention volume to PS-calibrated molecular weight was executed by Omnisec software native to the GPC instrument. Application of the polynomial correction was accomplished on Excel. This data was used to generate a continuous function that interconverts retention volume and molecular weight, which was required for modeling purposes. First, discrete retention volume points corresponding to actual polymer sizes (*i.e.* – polymer of n = 1 has MW = 84.16 Da, n = 2 has MW = 168.32 Da, etc.) were selected from the bulk data using a macro written in Visual Basic. Using these discrete data, a plot of log molecular weight as a function of retention volume was created (Figure S4). Initially, attempts were made to fit the data with a single continuous function (equation S3 where a = -1.83746 and b = 23.229), but this did not provide a good fit of the data, especially at late retention volumes (Figure S1). Nevertheless, an acceptable fit was obtained using a semi-continuous function consisting of

multiple spliced log functions, where a = -1.4345 and b = 21.829 for MW = 0 – 3787 Da; a = -1.6901 and b = 22.741 for MW = 3787 – 18936 Da; a = -1.9756 and b = 23.961 for MW = 18936 – 55966 Da; a = -2.1806 and b = 24.934 for MW = 55966 Da and above.

$$RV = aLog(MW) + b \quad \text{(S3)}$$

Despite our best efforts in calibration, small errors associated with the retention volume influence the accuracy of the molecular weight, particularly at early retention volumes due to the logarithmic molecular weight relationship. For example, a retention volume deviance of ± 0.1 mL (roughly the instrumental error) at 13.6 mL retention volume corresponds to a molecular weight deviation of ± 1354 Da or approximately 16 monomer insertions. To minimize these errors we model all kinetic data in retention volume or logarithmic molecular weight space rather than molecular weight space. Furthermore, this specific GPC column and PS-calibration standard are most accurate for molecular weights between 500 and 100000 Da. So data above 18 mL and below 14 mL retention volume are not reliable.

Inter-detector Delay:

After eluting through the GPC, the sample is sent through the UV detector before arriving at the RI detector, leading to a slight inter-detector delay. Indeed, UV and RI signals are slightly misaligned in the raw data. Aligning the UV and RI signals by adjusting the UV retention volume in Excel for the five-point narrow PS standard revealed that the UV signal is 0.147 ± 0.011 mL premature at the standard 1.0 mL/min flow rate. All UV data was adjusted to match the RI since the absolute molecular weight calibrations are based on the RI signal.

Broadening of Discrete GPC bands into a Continuous Distribution:

Figures S5 depicts an ideal GPC chromatograph in the absence of band broadening where each line represents a species of discrete and different mass, and as shown above in Figure S4, the relationship between molecular weight and retention volume is nearly logarithmic with higher molecular weight material eluting at earlier retention volumes. Due to non-perfect sample elution, each species is broadened such that each line transforms into a roughly Gaussian distribution (Figure S6). Since band broadening is greater than the difference in retention volumes of each species, particularly for large molecular weight polymers, significant sample overlap occurs at early retention volumes. The observed GPC chromatograph is the sum of all the discrete, Gaussian-broadened lines, where the overlap relationships distort the overall shape to emphasize the signal at early retention volume (Figure S7). As described in the text, band-broadening was modeled either by replicating this phenomenon by convolution of the polymer concentrations at each molecular that were obtained from a kinetic model with an exponentially modified Gaussian functions (EMG).

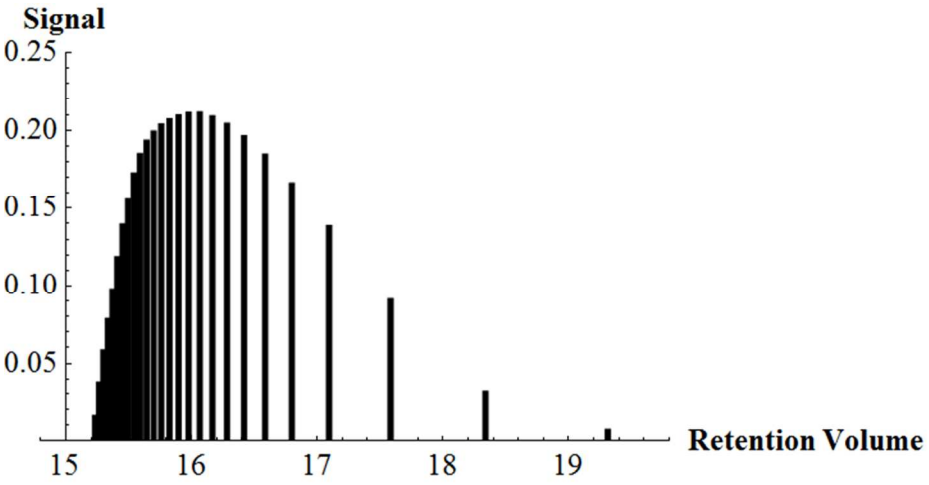

Figure S5: Example of an expected GPC chromatogram in the absence of band broadening.

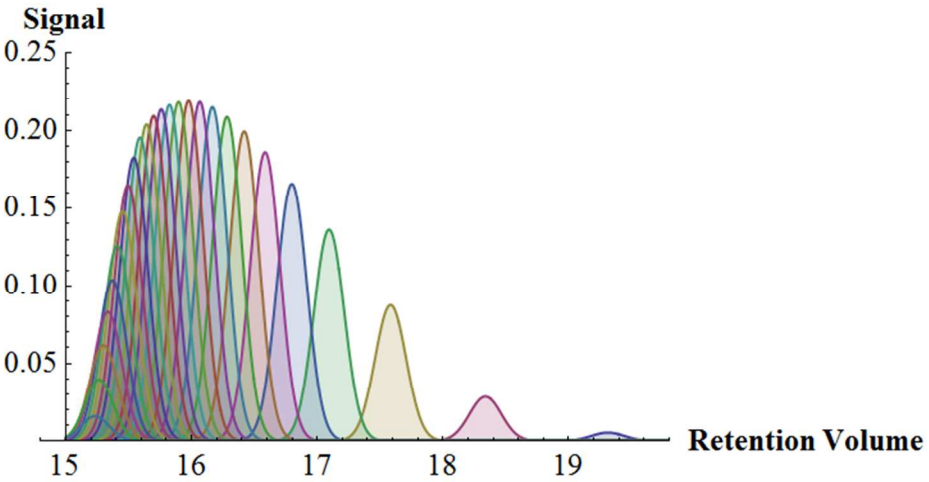

Figure S6: Depicted exponentially-modified gaussian (EMG) broadening of each individual species.

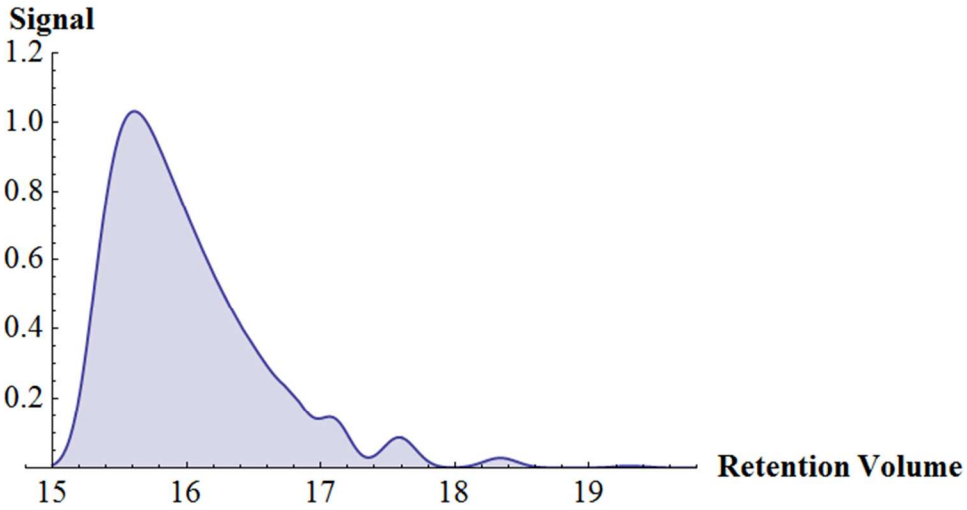

Figure S7: Example of an observed GPC chromatogram after convolution with the EMG. Note the increase in signal intensity at early retention volumes relative to those in the two previous figures.

Data Weighting:

When modeling multiple heterogeneous data, it is necessary to weight the data so that each data source is fairly represented in the modeling program. Attempting to fit data in the absence of data weighing will bias the fit in favor data with the largest absolute values, since deviations in these parameters will likewise have largest nominal value. However, caution must be taken when weighing data to avoid untoward human bias. To ensure that human biases are not reflected in the results, four different weighting schemes were implemented in this study. Weighting by 1/variance or value/variance are common practice. Initially, UV and RI data were weighed evenly at all points. However, since precision and accuracy of the data are not the same at all retention volumes (*vide supra*), we implemented two weighting schemes that apply different weights to the individual points of the MWD data. Assuming that errors are largest in the high retention volumes, these weighting schemes weight the RI and UV data as a function of polymer mass or the square of polymer mass. Although this assumption is not strictly correct, these schemes will serve to reveal the importance of individually weighting the MWD. Note: the model used to fit the data here did not take catalyst death or unlabeled quenching (*vide infra*) into account.

The average resolved rate constants for each weighting scheme, shown in Table S1, demonstrate that average resolved values are the same within error. Thus, human biases did not play a role during kinetic fitting, and the data is robust enough so that it is not dramatically dependent on the weighting.

TABLE S1. Average rate constants resolved using different weighting schemes. Fitting was done without making any assumptions of catalyst death or unlabeled quenching.

Weighting Scheme	k_i ($M^{-1}s^{-1}$)	k_p ($M^{-1}s^{-1}$)	$k_{1,2}$ (s^{-1})	$k_{2,1}$ ($M^{-1}s^{-1}$)	k_r ($M^{-1}s^{-1}$)
1/variance	0.027 ± 0.010	2.9 ± 0.4	0.0027 ± 0.0006	0.010 ± 0.001	0.09 ± 0.08
value/variance	0.030 ± 0.007	3.0 ± 0.4	0.0026 ± 0.0003	0.011 ± 0.002	0.13 ± 0.12
value/variance – MW dependent	0.031 ± 0.007	3.0 ± 0.5	0.0027 ± 0.0003	0.011 ± 0.002	0.14 ± 0.11
value/variance – MW^2 dependent	0.032 ± 0.008	3.0 ± 0.5	0.0028 ± 0.00036	0.011 ± 0.002	0.10 ± 0.08

Unlabeled Quenching versus Catalyst Death Prior to Reaction

Active site counts as revealed by chromophore labeling were measured at different initial concentrations of catalyst. The plot of active site concentration vs. the added catalyst concentration is well described by a straight line with an x-intercept of 0.15 mM (Figure S8) and a slope (0.93) slightly less than one. The two most likely causes for the positive, non-zero x-intercept are either (1) quenching without labeling, perhaps caused by

impurities in the quenching agent, or (2) catalyst death prior to reaction, caused by impurities introduced by other sources such as the solvent or alkene.

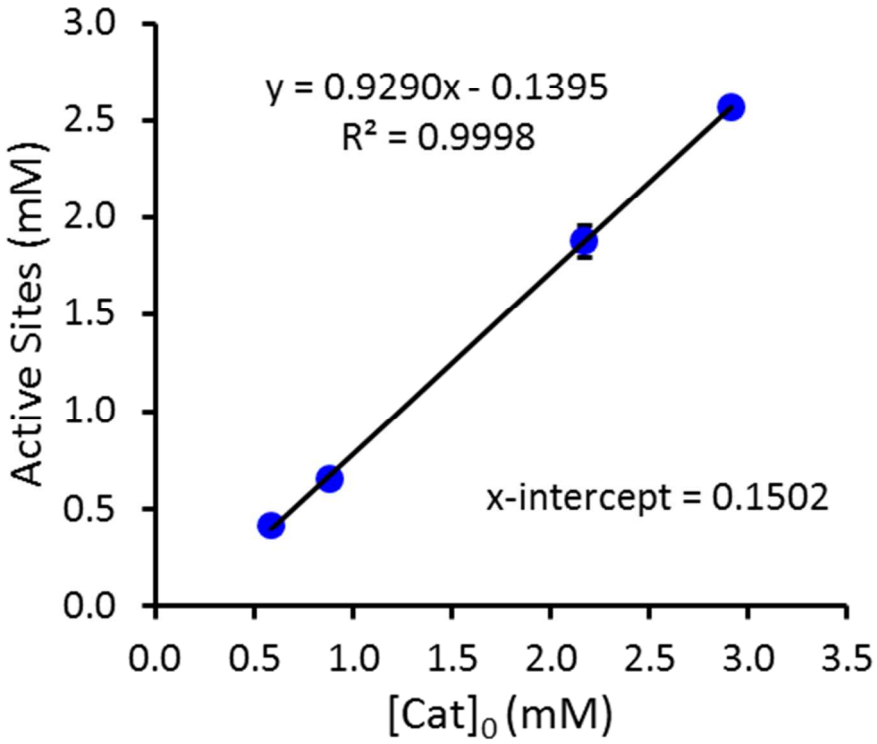

Figure S8. Maximum active site count as a function of initial catalyst concentration. All reactions performed with [1-hexene]$_0$=1.0 M at 0°C in toluene solution. Error bars, which are shown at the only catalyst concentration with multiple data sets, represent 95% confidence.

We evaluate the validity of each hypothesis using kinetic modeling. The "early catalyst death" hypothesis was simulated by subtracting 0.15 mM from the initial catalyst concentration and fitting all kinetic parameters to observed data. The hypothesis of "unlabeled quenching" was tested by adding 0.15 mM universally to the observed active site data followed by fitting the kinetic parameters to the observed data. These two treatments were modeled at the lowest catalyst concentrations, [cat]$_0$ = 0.583 mM and [cat]$_0$ = 0.879 mM, since these data points will be most sensitive to 0.15 mM adjustments. After parameter optimization, the quality of each fit was assessed by comparing objective functions (the sum of square deviations between computed and observed data) and the rate constants and estimated errors (Table S2). The rate constants for the two hypothetical tests were further compared against the average rate constants obtained when all data were used in the fitting procedures (i. e., the data obtained with [cat]$_0$ = 2.17 mM and [cat]$_0$ = 2.91 mM were included). Our assumption is that the fits obtained when data obtained using the two higher concentrations of catalyst will be less affected by small corrections in the active catalyst concentration. Objective functions for the model of "early catalyst death" and the original, unmodified models are nearly equal. These objective functions are lower than those for the "unlabeled quenching" model, indicating that the unlabeled quenching model poorly fits the data. Comparing the rate constants reveals considerable deviations in k_i and k_r, with the catalyst death model predicting values closer to the expected amounts (*i.e.* – those in Entry 1). Thus, these analyses suggest that the "early catalyst death" model best

fits the data; systematic impurities in the reaction solution apparently lead to significant catalyst death prior to catalysis.

Table S2. Results of kinetic modeling that compared the original model, catalyst death model, and unlabeled quenching model.

Entry	[cat] mM	Model	k_i ($M^{-1}s^{-1}$)	k_r ($M^{-1}s^{-1}$)	Objective
1	2.17 and 2.91	original	0.032 ± 0.008	0.13 ± 0.8	n/a
2	0.583	original	0.190	0.024	4.106×10^{-9}
3	0.583	catalyst death	0.0257	0.11	4.088×10^{-9}
4	0.583	unlabeled quenching	0.0146	0.116	7.658×10^{-9}
5	0.879	original	0.017	0.020	9.246×10^{-8}
6	0.879	catalyst death	0.021	0.041	9.258×10^{-8}
7	0.879	unlabeled quenching	0.019	0.026	10.01×10^{-8}

Fits of the Data Using Optimized Rate Constants

EMG Treatment Overall Average

k_i = 0.029 ± 0.008 $M^{-1}s^{-1}$
k_p = 2.9 ± 0.3 $M^{-1}s^{-1}$
k_{12} = 0.0027 ± 0.0006 s^{-1}
k_{21} = 0.010 ± 0.001 $M^{-1}s^{-1}$
k_r = 0.11 ± 0.07 $M^{-1}s^{-1}$

Unit Conversion Treatment Overall Average

k_i = 0.028 ± 0.006 $M^{-1}s^{-1}$
k_p = 2.6 ± 0.4 $M^{-1}s^{-1}$
k_{12} = 0.0028 ± 0.0006 s^{-1}
k_{21} = 0.010 ± 0.001 $M^{-1}s^{-1}$
k_r = 0.15 ± 0.16 $M^{-1}s^{-1}$

0.583 mM catalyst

k_i = 0.0257 ± 0.005 $M^{-1}s^{-1}$
k_p = 2.34 ± 0.02 $M^{-1}s^{-1}$
k_{12} = 0.0018 ± 0.0001 s^{-1}
k_{21} = 0.0090 ± 0.0003 $M^{-1}s^{-1}$
k_r = 0.11 ± 0.02 $M^{-1}s^{-1}$

k_i = 0.037 ± 0.002 $M^{-1}s^{-1}$
k_p = 2.01 ± 0.05 $M^{-1}s^{-1}$
k_{12} = 0.002 ± 0.005 s^{-1}
k_{21} = 0.008 ± 0.006 $M^{-1}s^{-1}$
k_r = 0.08 ± 0.06 $M^{-1}s^{-1}$

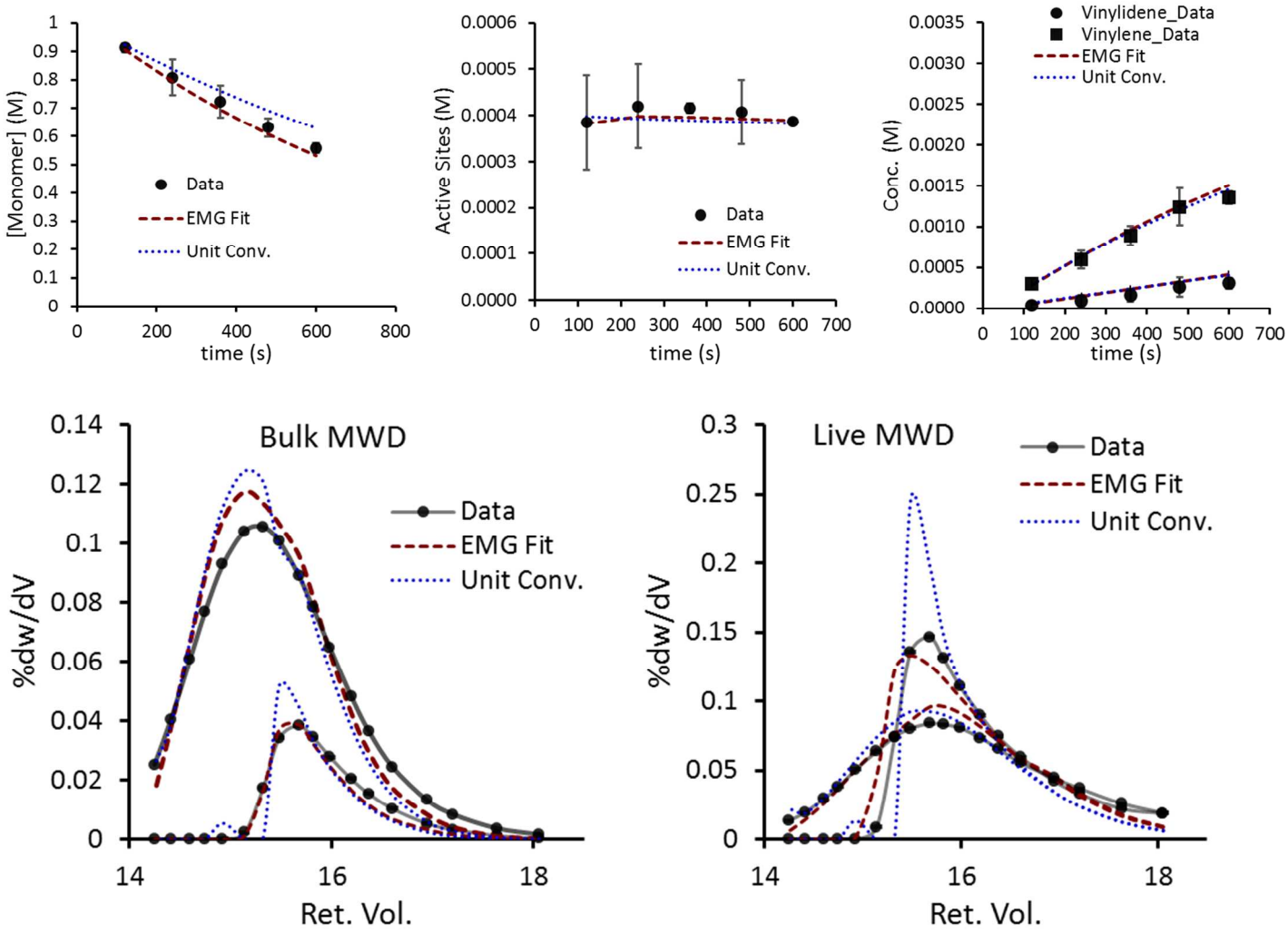

Figure S9: Data, EMG fit, and unit conversion fit for the time-course monomer consumption, active site, end-group concentration, Bulk MWD, and Live MWD for reactions with [hexene]0 = 1.0 M and [catalyst]0 = 0.583 mM (expected) at 0 °C.

Initial catalyst concentration was adjusted to 0.433 mM in the model. MWD data depicts only two sets of traces (at 120s and 600s) for clarity.

0.879 mM catalyst

k_i = 0.021 ± 0.001 $M^{-1}s^{-1}$
k_p = 2.54 ± 0.04 $M^{-1}s^{-1}$
k_{12} = 0.002 ± 0.001 s^{-1}
k_{21} = 0.009 ± 0.002 $M^{-1}s^{-1}$
k_r = 0.041 ± 0.004 $M^{-1}s^{-1}$

k_i = 0.0257 ± 0.0001 $M^{-1}s^{-1}$
k_p = 2.417 ± 0.001 $M^{-1}s^{-1}$
k_{12} = 0.002 ± 0.001 s^{-1}
k_{21} = 0.009 ± 0.002 $M^{-1}s^{-1}$
k_r = 0.032 ± 0.003 $M^{-1}s^{-1}$

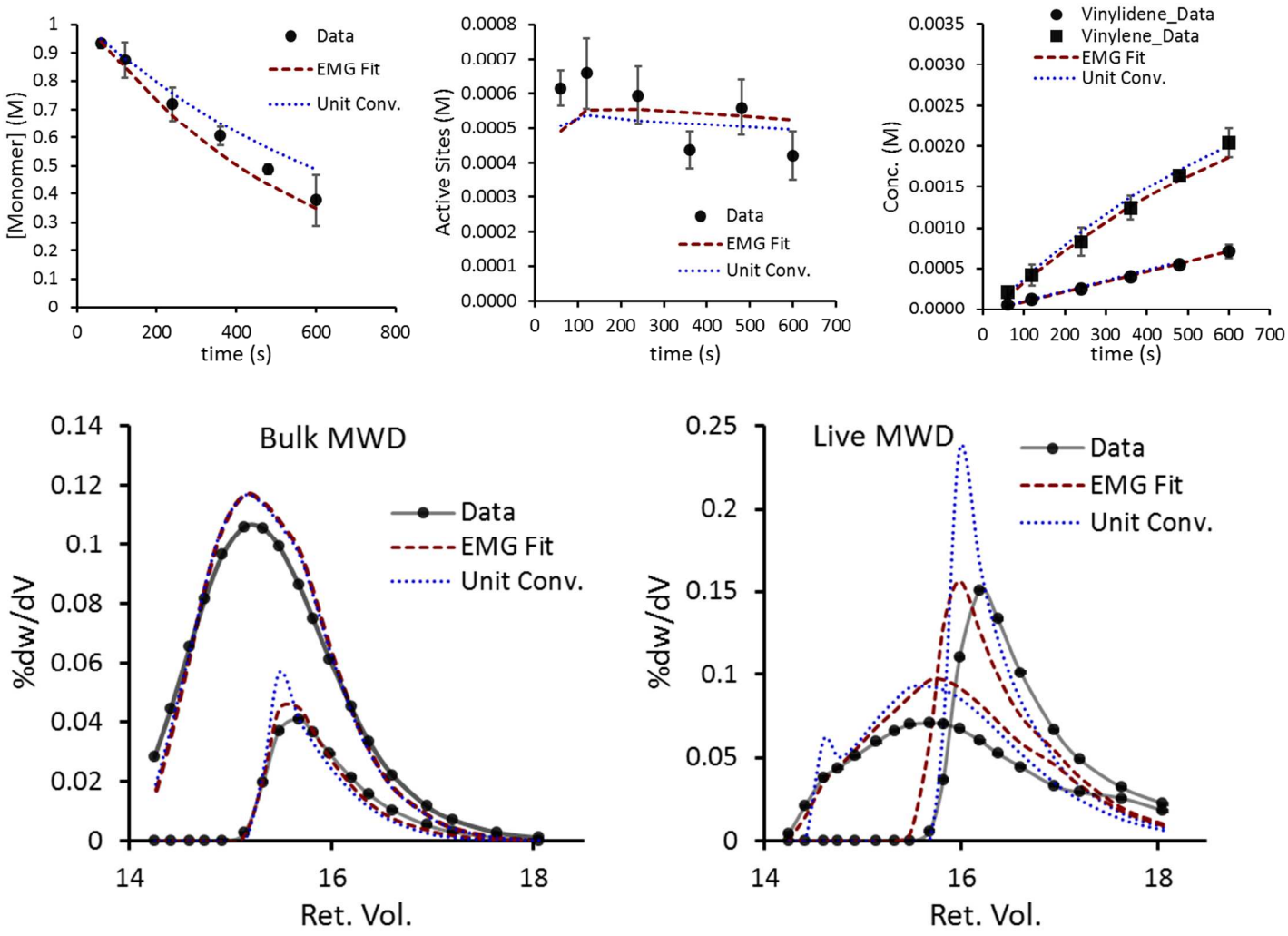

Figure S10: Data, EMG fit, and unit conversion fit for the time-course monomer consumption, active site, end-group concentration, Bulk MWD, and Live MWD for reactions with [hexene]0 = 1.0 M and [catalyst]0 = 0.879 mM (expected) at 0 °C. Initial catalyst concentration was adjusted to 0.729 mM in the model. MWD data depicts only two sets of traces (at 120s and 600s) for clarity.

2.91 mM catalyst

$k_i = 0.034 \pm 0.002\ M^{-1}s^{-1}$
$k_p = 3.24 \pm 0.04\ M^{-1}s^{-1}$
$k_{12} = 0.0032 \pm 0.0007\ s^{-1}$
$k_{21} = 0.012 \pm 0.002\ M^{-1}s^{-1}$
$k_r = 0.24 \pm 0.09\ M^{-1}s^{-1}$

$k_i = 0.030 \pm 0.002\ M^{-1}s^{-1}$
$k_p = 3.05 \pm 0.03\ M^{-1}s^{-1}$
$k_{12} = 0.003 \pm 0.001\ s^{-1}$
$k_{21} = 0.012 \pm 0.002\ M^{-1}s^{-1}$
$k_r = 0.4 \pm 0.3\ M^{-1}s^{-1}$

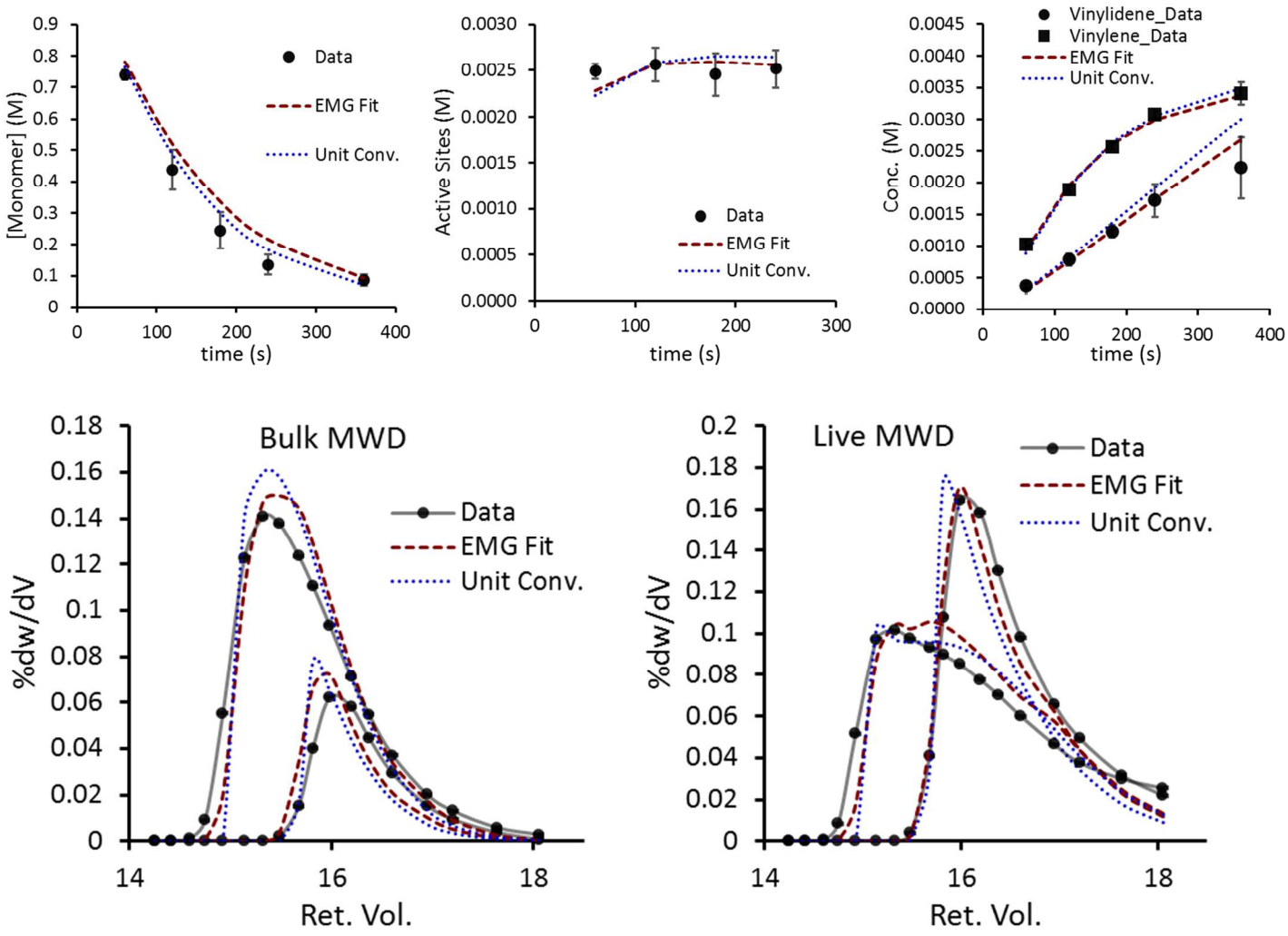

Figure S11: Data, EMG fit, and unit conversion fit for the time-course monomer consumption, active site, end-group concentration, Bulk MWD, and Live MWD for reactions with [hexene]0 = 1.0 M and [catalyst]0 = 2.91 mM at 0 °C. MWD data depicts only two sets of traces (at 60s and 240s) for clarity.

0.5 M hexene

$k_i = 0.042 \pm 0.004$ $M^{-1}s^{-1}$
$k_p = 3.13 \pm 0.04$ $M^{-1}s^{-1}$
$k_{12} = 0.0032 \pm 0.0007$ s^{-1}
$k_{21} = 0.012 \pm 0.002$ $M^{-1}s^{-1}$
$k_r = 0.13 \pm 0.05$ $M^{-1}s^{-1}$

$k_i = 0.035 \pm 0.004$ $M^{-1}s^{-1}$
$k_p = 2.87 \pm 0.04$ $M^{-1}s^{-1}$
$k_{12} = 0.003 \pm 0.002$ s^{-1}
$k_{21} = 0.012 \pm 0.002$ $M^{-1}s^{-1}$
$k_r = 0.4 \pm 0.5$ $M^{-1}s^{-1}$

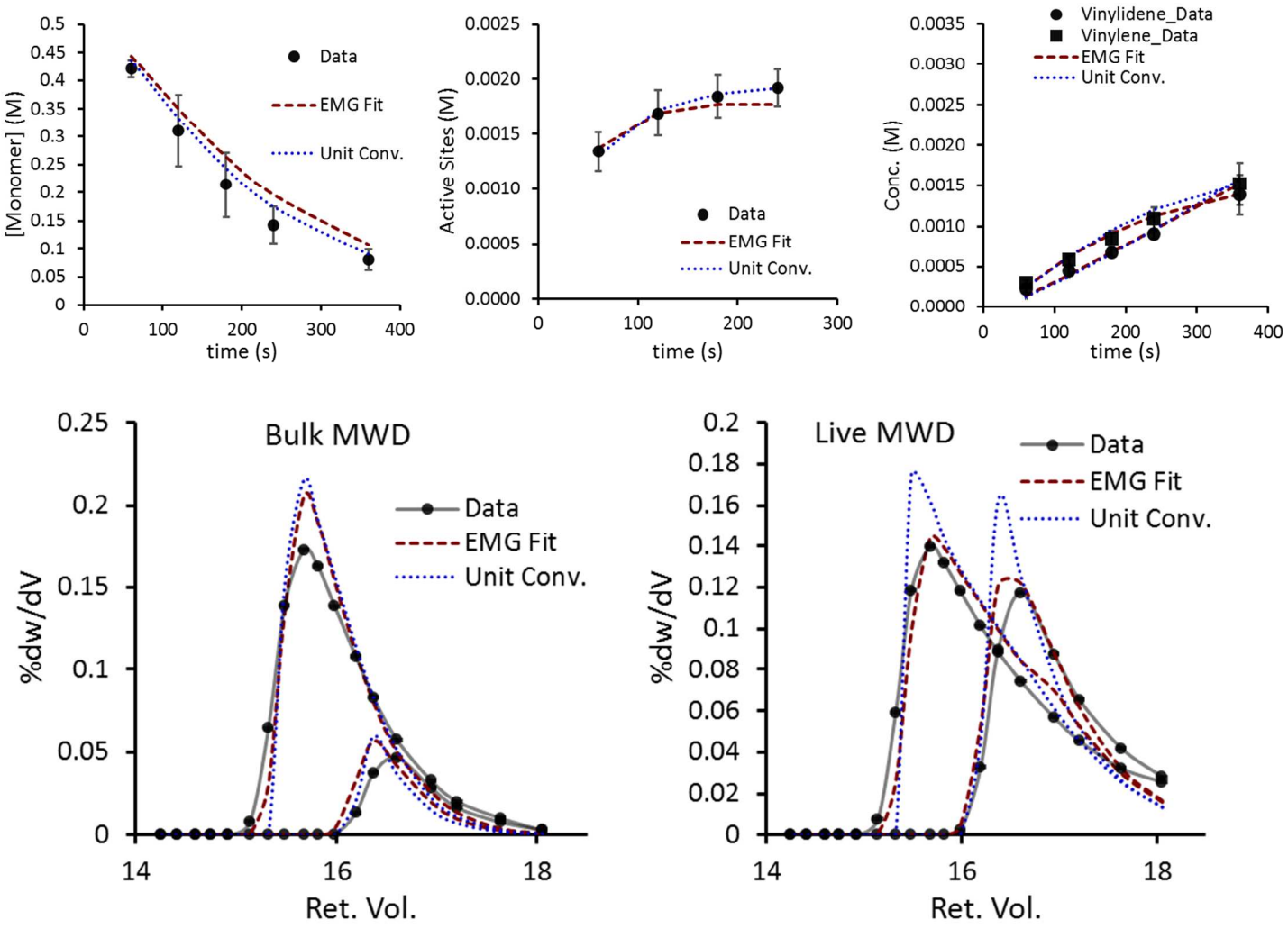

Figure S12: Data, EMG fit, and unit conversion fit for the time-course monomer consumption, active site, end-group concentration, Bulk MWD, and Live MWD for reactions with [hexene]0 = 0.5 M and [catalyst]0 = 2.17 mM at 0 °C. MWD data depicts only two sets of traces (at 60s and 240s) for clarity.

1.0 M hexene

$k_i = 0.024 \pm 0.003$ $M^{-1}s^{-1}$
$k_p = 2.99 \pm 0.05$ $M^{-1}s^{-1}$
$k_{12} = 0.003 \pm 0.002$ s^{-1}
$k_{21} = 0.011 \pm 0.003$ $M^{-1}s^{-1}$
$k_r = 0.06 \pm 0.02$ $M^{-1}s^{-1}$

$k_i = 0.023 \pm 0.003$ $M^{-1}s^{-1}$
$k_p = 2.71 \pm 0.04$ $M^{-1}s^{-1}$
$k_{12} = 0.003 \pm 0.004$ s^{-1}
$k_{21} = 0.012 \pm 0.006$ $M^{-1}s^{-1}$
$k_r = 0.05 \pm 0.01$ $M^{-1}s^{-1}$

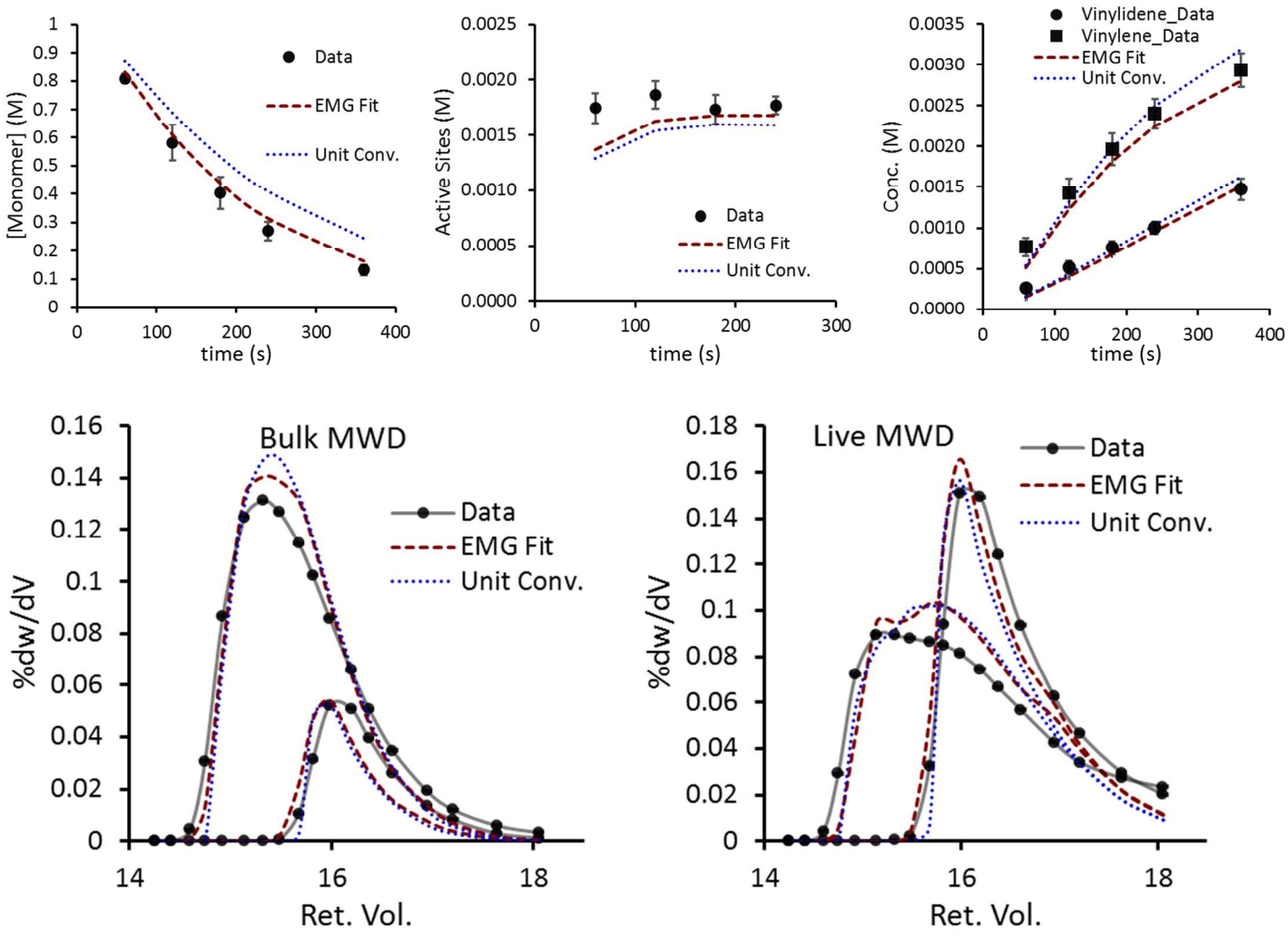

Figure S13: Data, EMG fit, and unit conversion fit for the time-course monomer consumption, active site, end-group concentration, Bulk MWD, and Live MWD for reactions with [hexene]0 = 1.0 M and [catalyst]0 = 2.17 mM at 0 °C. MWD data depicts only two sets of traces (at 60s and 240s) for clarity.

1.5 M hexene

$k_i = 0.027 \pm 0.003\ M^{-1}s^{-1}$
$k_p = 3.07 \pm 0.06\ M^{-1}s^{-1}$
$k_{12} = 0.003 \pm 0.002\ s^{-1}$
$k_{21} = 0.011 \pm 0.002\ M^{-1}s^{-1}$
$k_r = 0.07 \pm 0.01\ M^{-1}s^{-1}$

$k_i = 0.022 \pm 0.002\ M^{-1}s^{-1}$
$k_p = 2.97 \pm 0.04\ M^{-1}s^{-1}$
$k_{12} = 0.003 \pm 0.002\ s^{-1}$
$k_{21} = 0.012 \pm 0.002\ M^{-1}s^{-1}$
$k_r = 0.10 \pm 0.02\ M^{-1}s^{-1}$

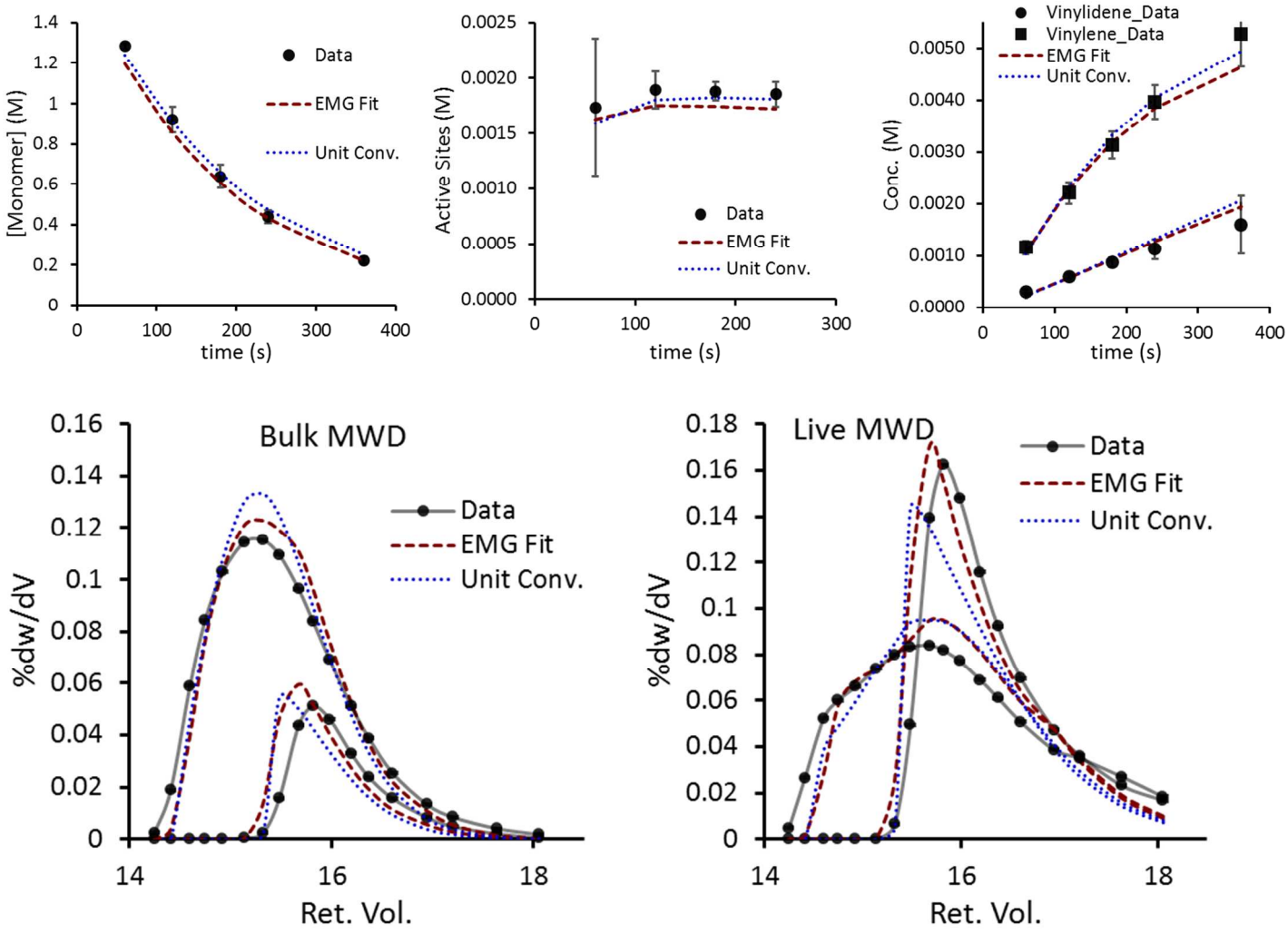

Figure S14: Data, EMG fit, and unit conversion fit for the time-course monomer consumption, active site, end-group concentration, Bulk MWD, and Live MWD for reactions with [hexene]0 = 1.5 M and [catalyst]0 = 2.17 mM at 0 °C. MWD data depicts only two sets of traces (at 60s and 240s) for clarity.

NMR Spectra

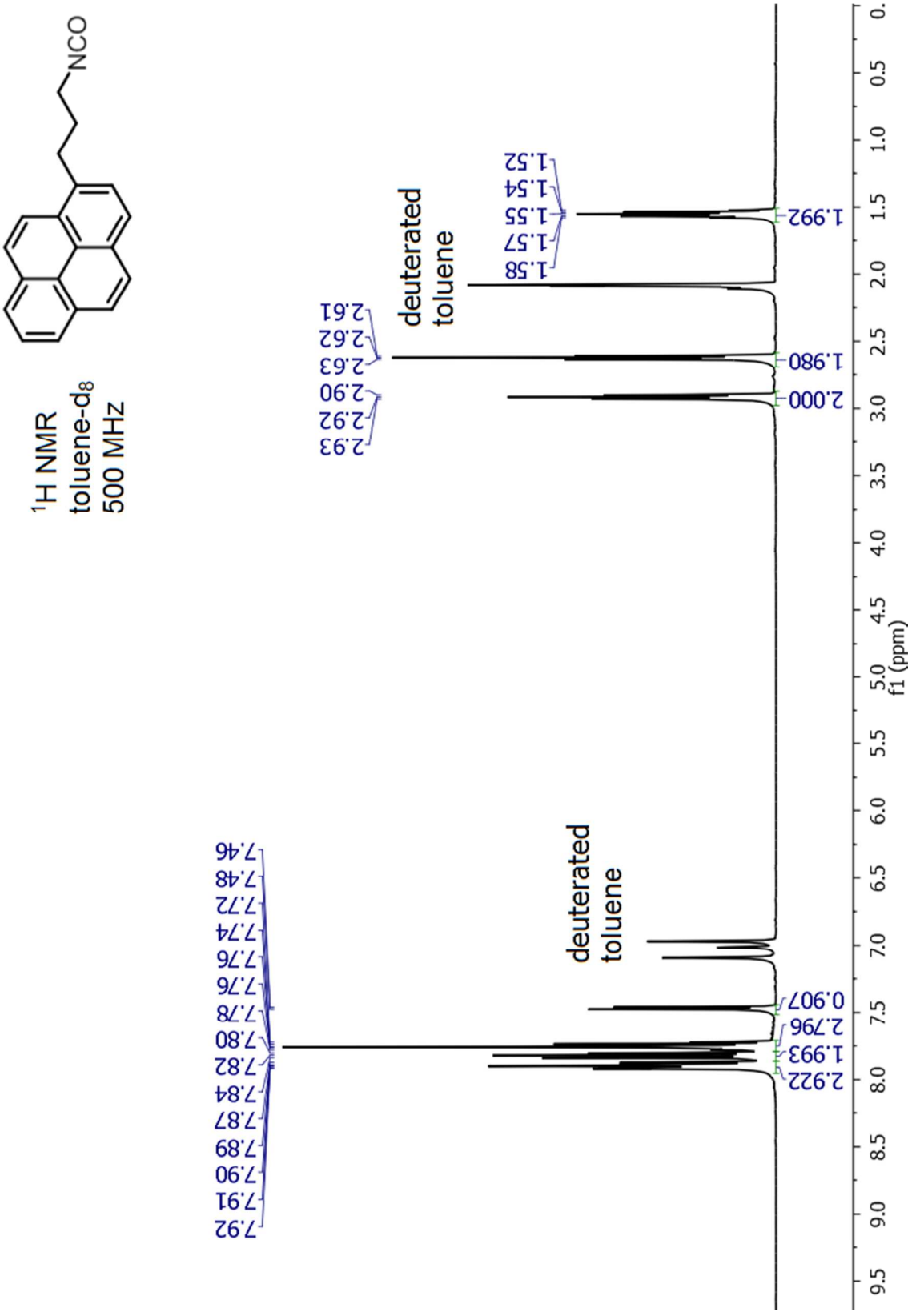

Figure S15: ^{1}H NMR spectra for **2** in toluene-d_8.

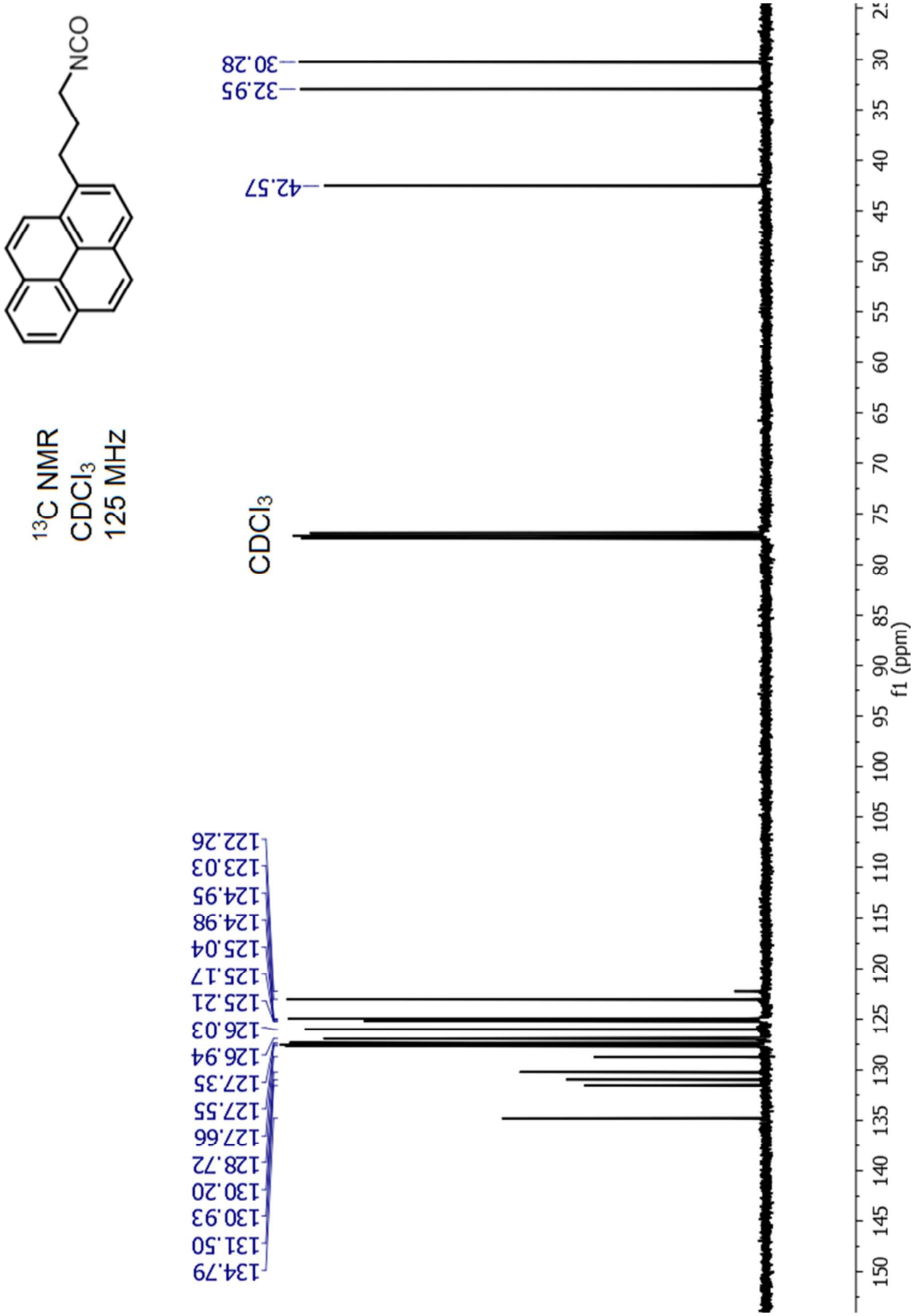

Figure S16: ^{13}C NMR spectra for **2** in $CDCl_3$.

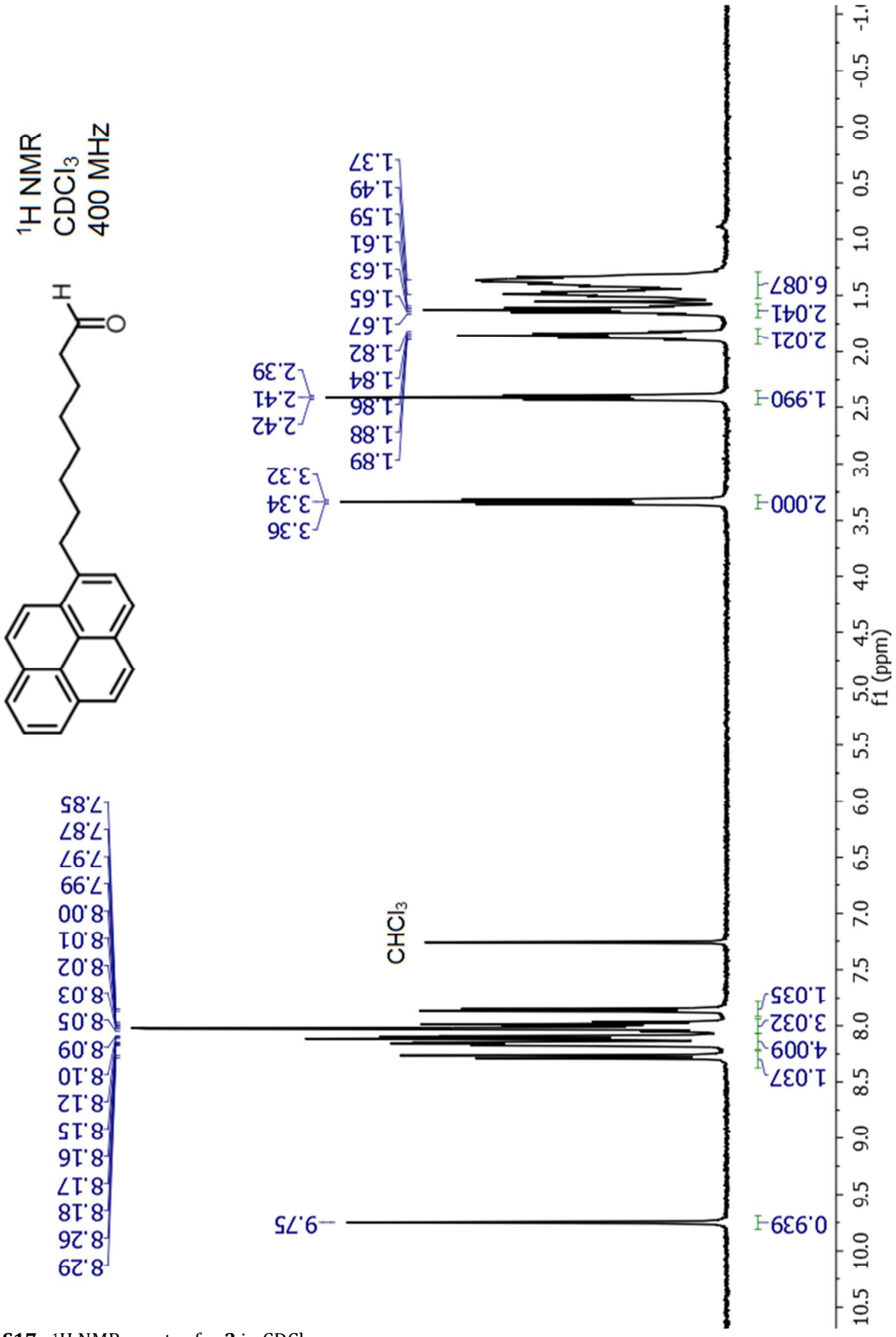

Figure S17: ^{1}H NMR spectra for **3** in $CDCl_3$.

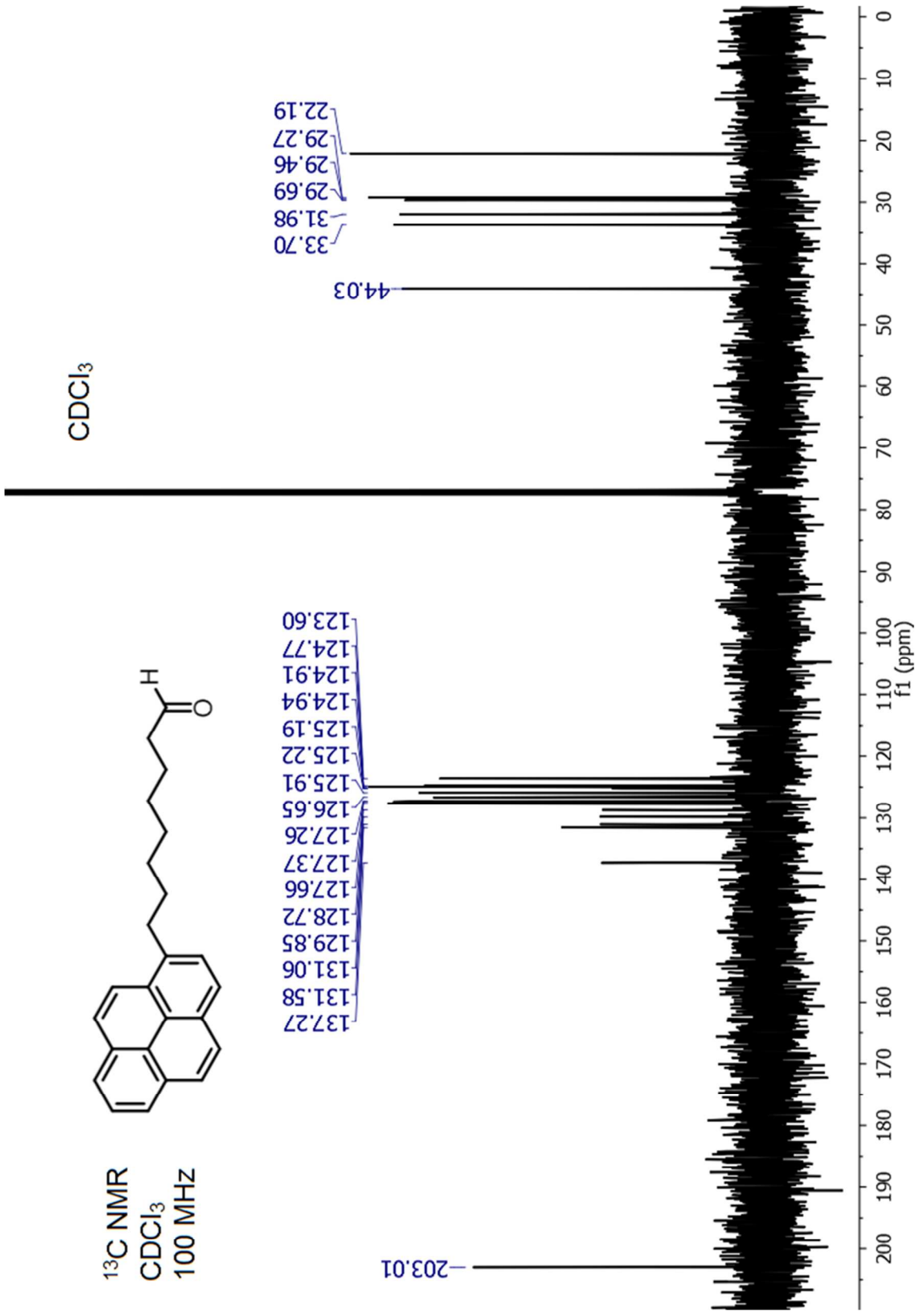

Figure S18: ^{13}C NMR spectra for **3** in $CDCl_3$.

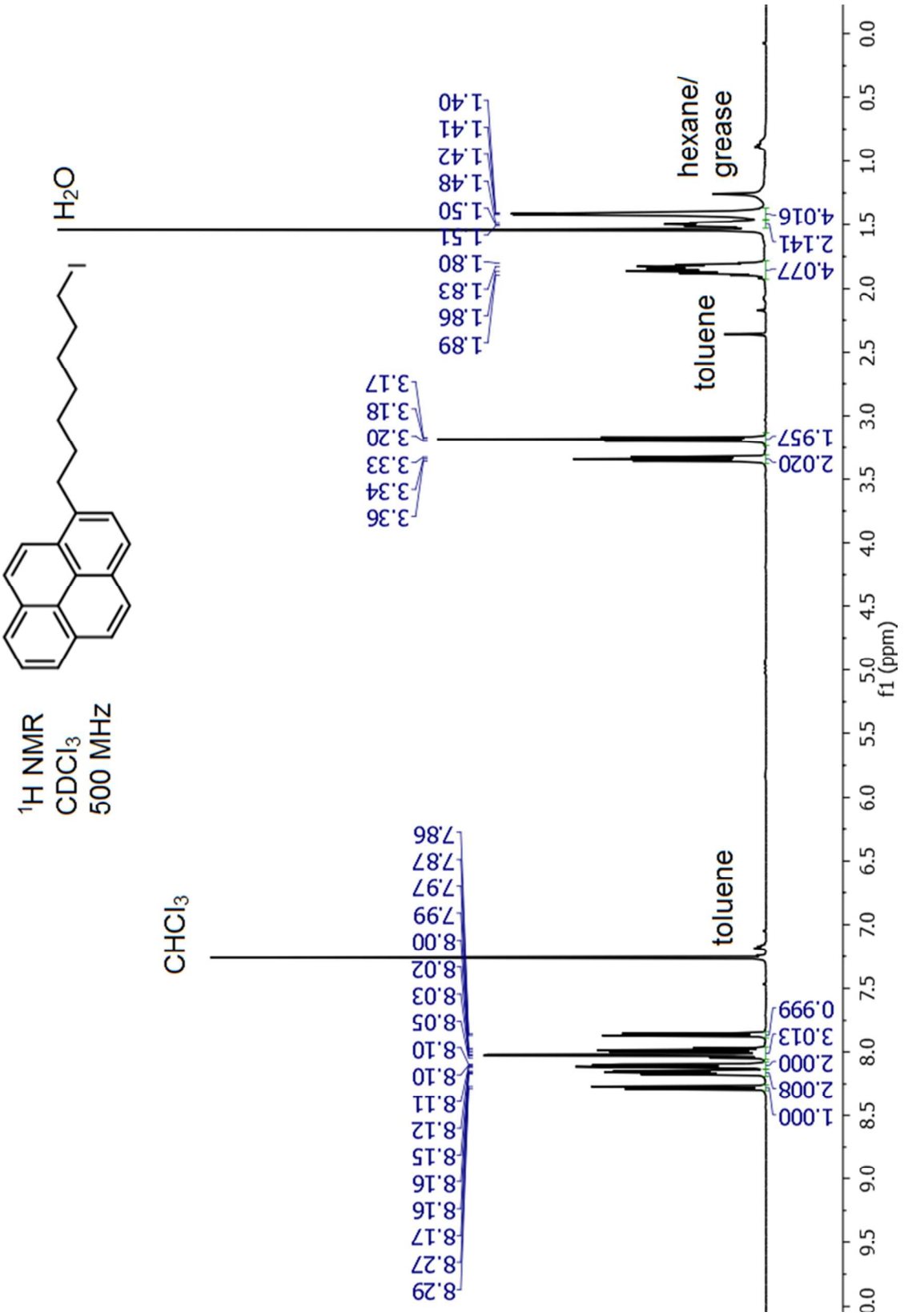

Figure S19: ^{1}H NMR spectra for **10** in $CDCl_3$.

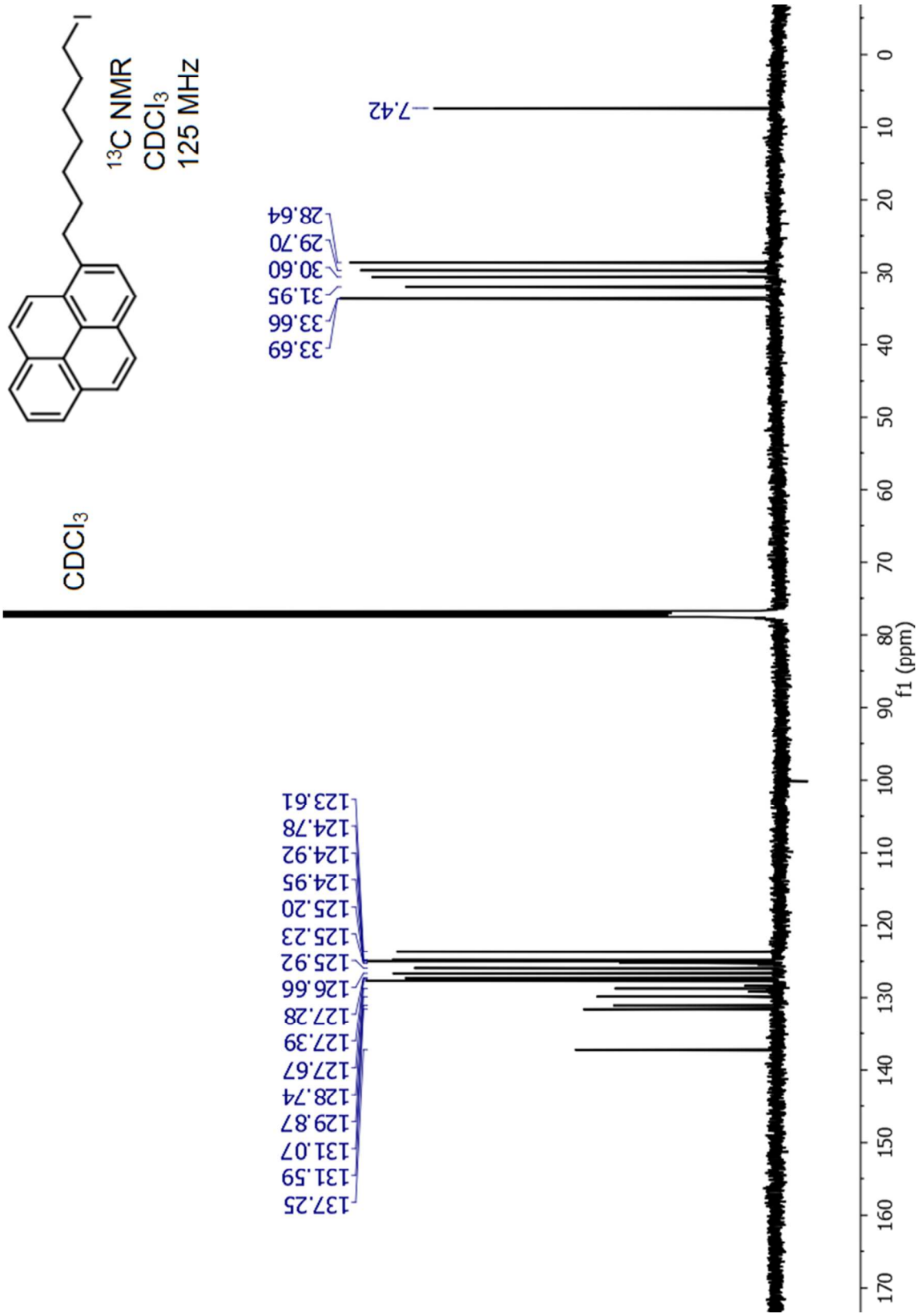

Figure S20: ^{13}C NMR spectra for **10** in $CDCl_3$.

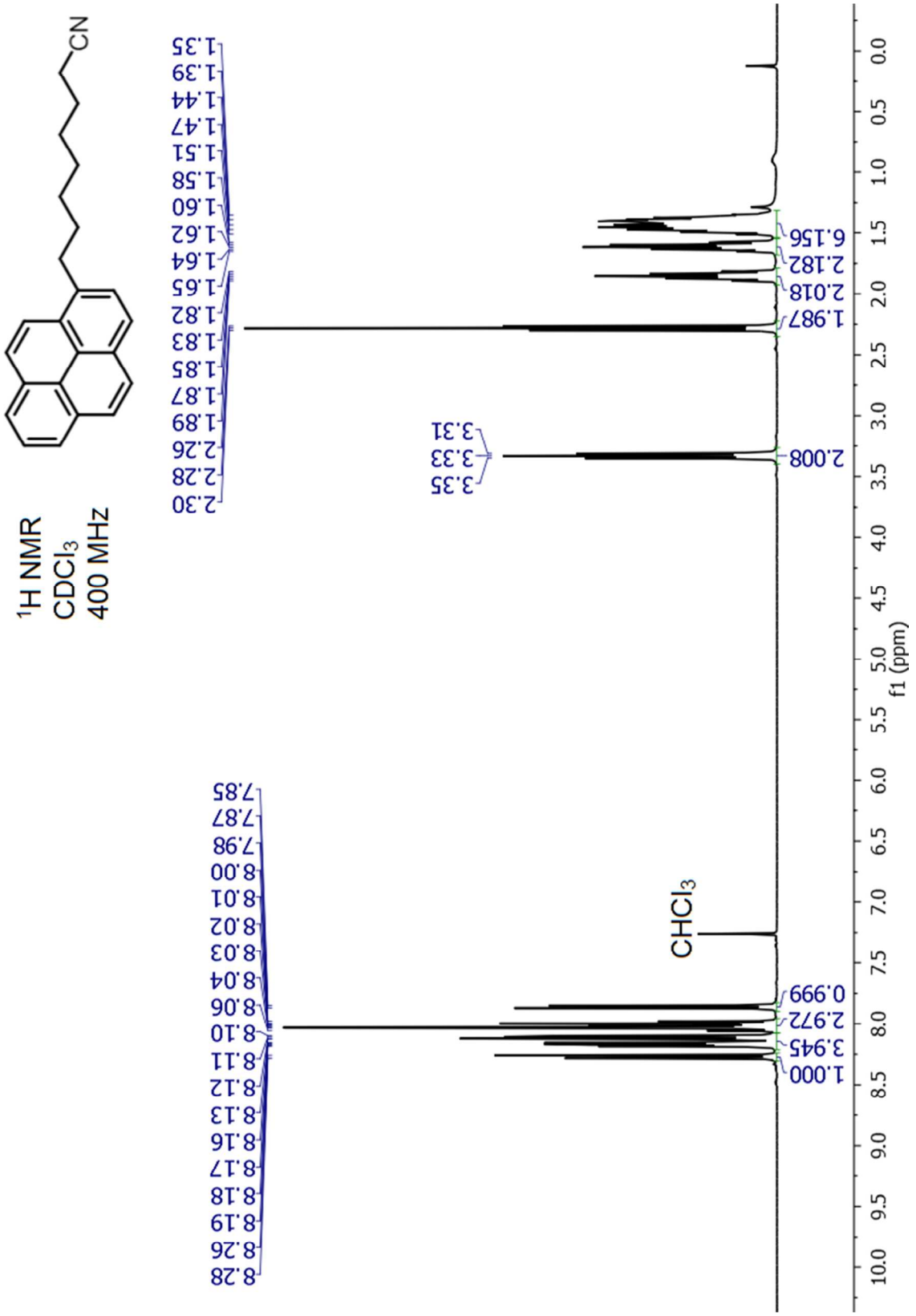

Figure S21: ^{1}H NMR spectra for **4** in $CDCl_3$.

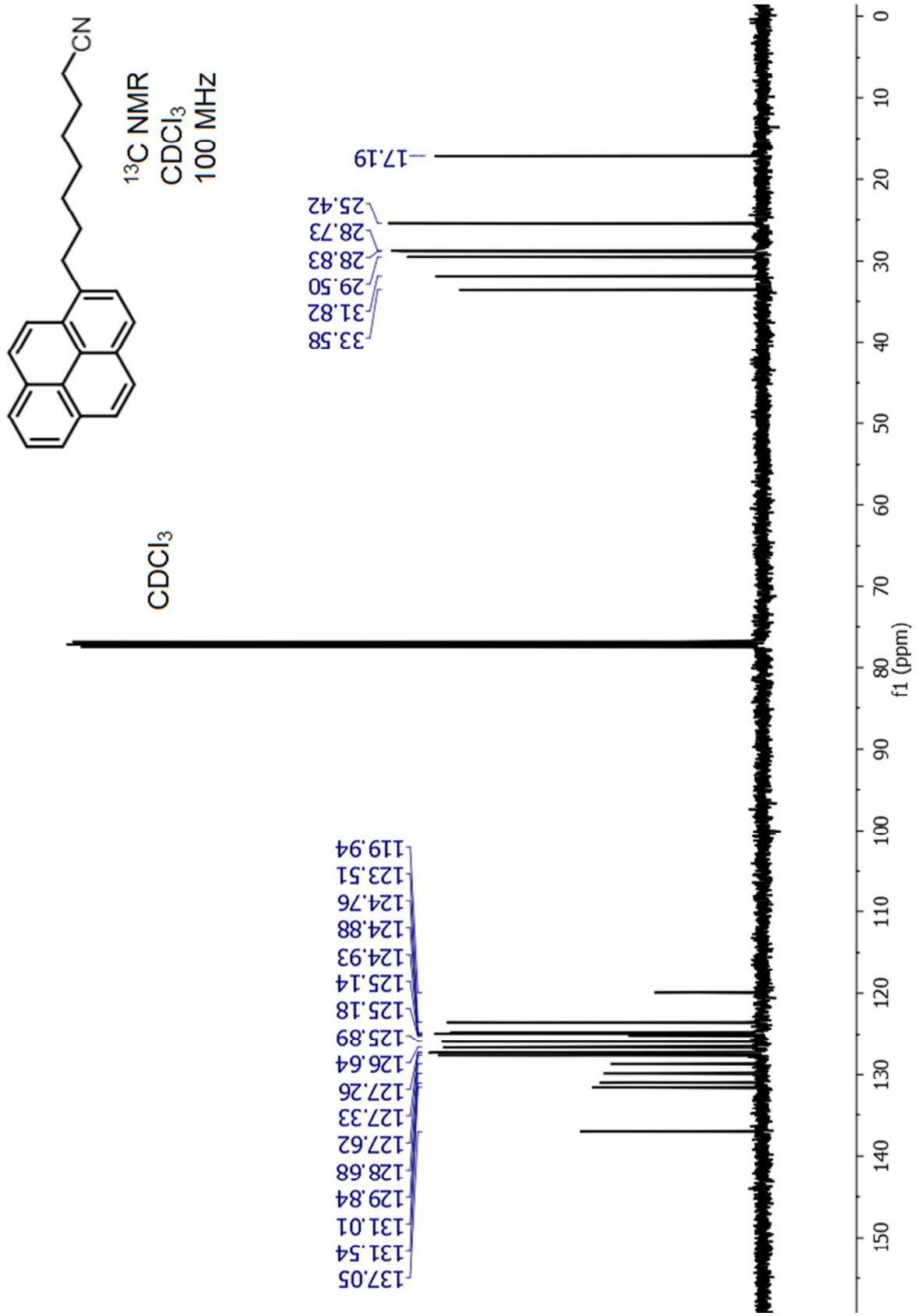

Figure S22: ^{13}C NMR spectra for **4** in $CDCl_3$.

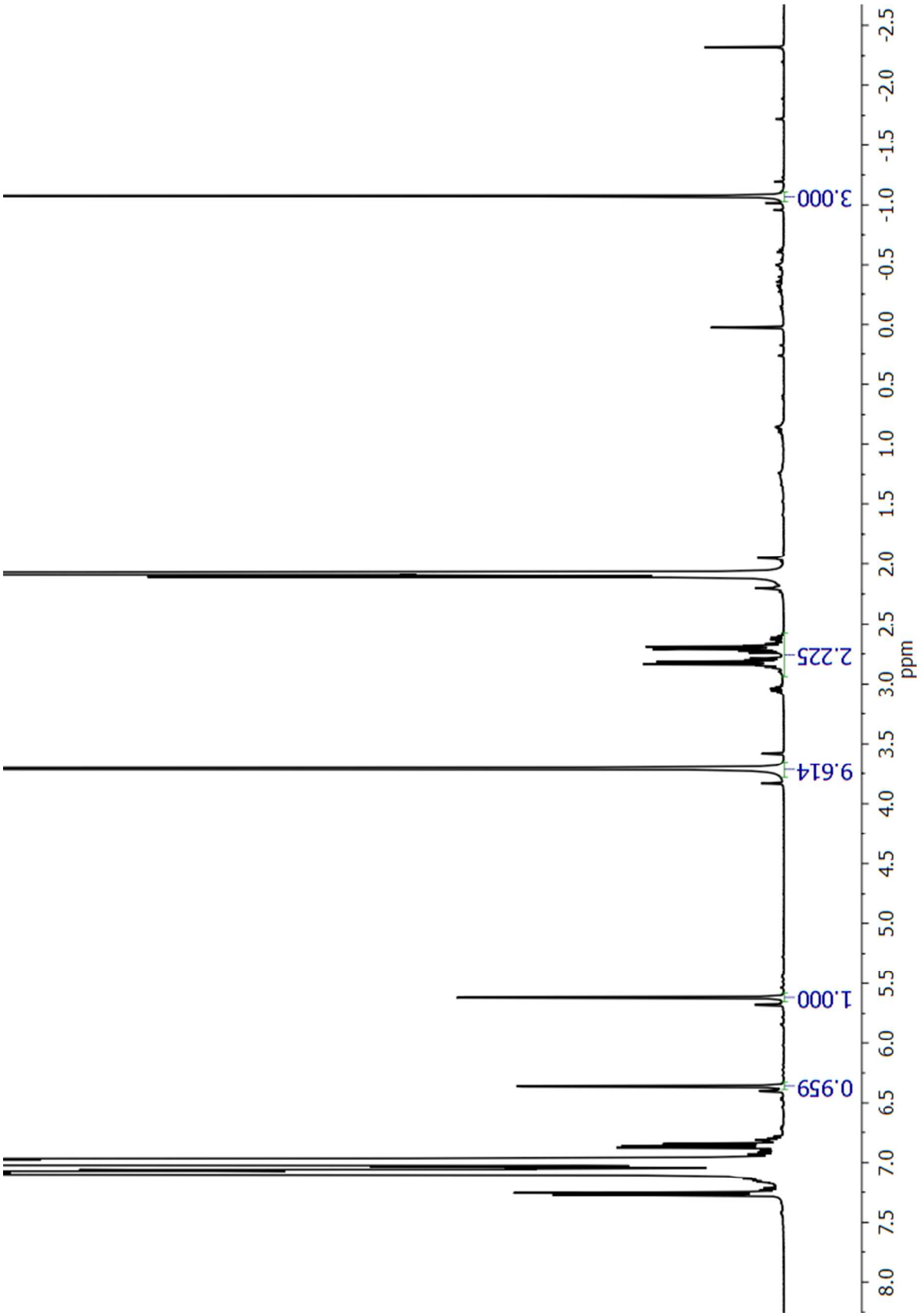

Figure S23: ^{1}H NMR spectra for (EBI)$ZrMe_2$ in d_8–toluene with diphenylmethane as internal integration standard. The potency of this sample is 90.3%.

Illustration of UV-Chromophore Sensitivity

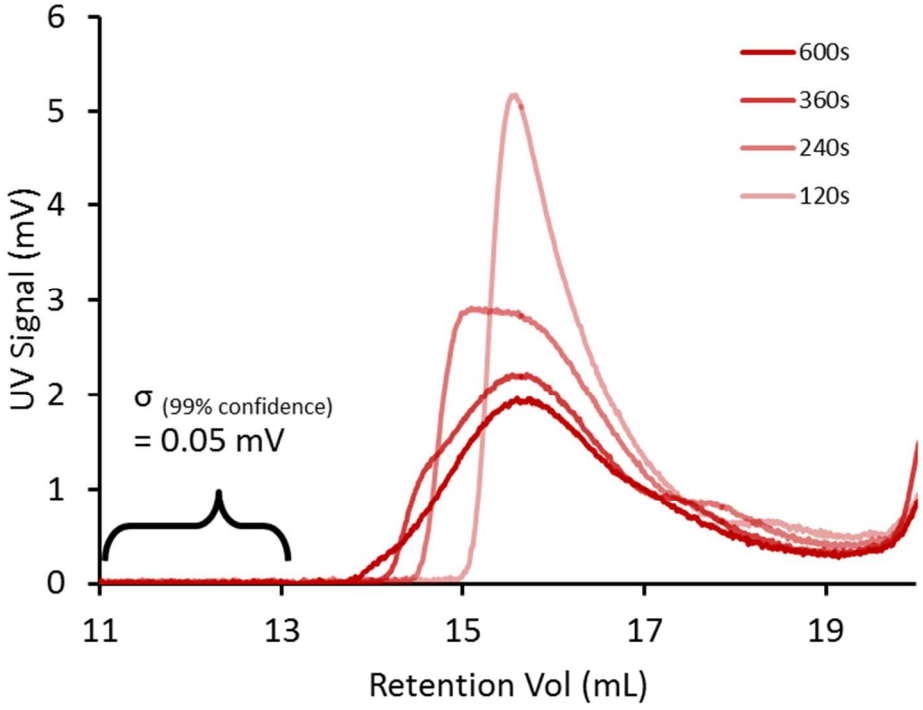

Figure S24: Illustration of the signal-to-noise of the chromophore-labeled polymers obtained with 1.0 M hexene and nominal 0.88 mM catalyst at three different reaction times. The area under the 600s curve corresponds to the broadest distribution and a total active site concentration of 392μM. The sensitivity-detection limits of the quench labeling method depend on the breadth of the labeled polymer MWD with narrow distributions yielding high signal-to-noise.

Table S3. Table of Data for Quench-Label Active Site Counts under different conditions. All data are run at least in duplicate.

Zr Active Sites

[Cat] (mM)	[hexene] (M)	time (s)	[Active Sites](M)	Stdev (M)	Active Sites (%)	Stdev (%)
2.17	1.00	60	0.00174	0.00013	80%	6%
2.17	1.00	120	0.00187	0.00012	86%	6%
2.17	1.00	180	0.00174	0.00013	80%	6%
2.17	1.00	240	0.00177	0.00008	81%	4%

SUMMARY	Active Site (%)	Stdev (%)
all data	75%	11%
excluding [cat] < 2 mM	82%	7%

2.17	**0.50**	**60**	**0.00134**	**0.00018**	**62%**	**8%**
2.17	**0.50**	**120**	**0.00169**	**0.00020**	**78%**	**9%**
2.17	**0.50**	**180**	**0.00184**	**0.00019**	**85%**	**9%**
2.17	**0.50**	**240**	**0.00192**	**0.00017**	**89%**	**8%**
2.17	**1.50**	**60**	**0.00161**	**0.00033**	**74%**	**15%**
2.17	**1.50**	**120**	**0.00183**	**0.00094**	**84%**	**43%**
2.17	**1.50**	**180**	**0.00184**	**0.00039**	**85%**	**18%**
2.17	**1.50**	**240**	**0.00181**	**0.00042**	**83%**	**19%**
2.91	**1.00**	**60**	**0.00249**	**0.00008**	**86%**	**3%**
2.91	**1.00**	**120**	**0.00257**	**0.00018**	**88%**	**6%**
2.91	**1.00**	**180**	**0.00246**	**0.00023**	**84%**	**8%**
2.91	**1.00**	**240**	**0.00252**	**0.00020**	**86%**	**7%**
0.88	**1.00**	**60**	**0.00062**	**0.00005**	**70%**	**6%**
0.88	**1.00**	**120**	**0.00066**	**0.00010**	**75%**	**11%**
0.88	**1.00**	**240**	**0.00059**	**0.00008**	**68%**	**9%**
0.88	**1.00**	**360**	**0.00044**	**0.00005**	**50%**	**6%**
0.88	**1.00**	**480**	**0.00056**	**0.00008**	**64%**	**9%**
0.88	**1.00**	**600**	**0.00042**	**0.00007**	**48%**	**8%**
0.58	**1.00**	**120**	**0.00039**	**0.00010**	**66%**	**17%**
0.58	**1.00**	**240**	**0.00042**	**0.00009**	**72%**	**16%**
0.58	**1.00**	**360**	**0.00042**	**0.00001**	**71%**	**2%**
0.58	**1.00**	**480**	**0.00041**	**0.00007**	**70%**	**12%**
0.58	**1.00**	**600**	**0.00039**	**0.00001**	**66%**	**1%**

Reference

[1] Moscato, B. M.; Zhu, B.; Landis, C. R. *J. Am. Chem. Soc.* **2010**, *132*, 14352.